

Journal of
Mechanics of
Materials and Structures

**COUPLED FINITE ELEMENT FOR THE NONLINEAR DYNAMIC
RESPONSE
OF ACTIVE PIEZOELECTRIC PLATES
UNDER THERMOELECTROMECHANICAL LOADS**

Dimitris Varelis and Dimitris Saravanos

Volume 4, N^o 7-8

September 2009

 mathematical sciences publishers

COUPLED FINITE ELEMENT FOR THE NONLINEAR DYNAMIC RESPONSE OF ACTIVE PIEZOELECTRIC PLATES UNDER THERMOELECTROMECHANICAL LOADS

DIMITRIS VARELIS AND DIMITRIS SARAVANOS

A theoretical framework is presented for analyzing the coupled nonlinear dynamic behavior of laminated piezoelectric composite plates subject to high thermoelectromechanical loadings. It incorporates coupling between mechanical, electric, and thermal governing equations and encompasses geometric nonlinearity effects due to large displacements and rotations. The mixed-field shear-layerwise plate laminate theory formulation is considered, thus degenerating the 3D electromechanical field to 2D nodal variables, and an eight-node coupled nonlinear plate element is developed. The discrete coupled nonlinear dynamic equations of motion are formulated, linearized, and numerically solved at each time step using the implicit Newmark scheme with a Newton–Raphson technique. Validation and evaluation cases on active laminated beams demonstrate the accuracy of the method and its robust capability to effectively predict the nonlinear dynamic response under time-dependent combined mechanical, thermal, and piezoelectric actuator loads. The results illustrate the capability of the method to simulate large amplitude vibrations and dynamic buckling phenomena in active piezocomposite plates. The influence of loading rates on the nonlinear dynamic structural response is also quantified. Additional numerical cases demonstrate the complex dynamic interactions between electrical, mechanical, and thermal buckling loads.

1. Introduction

In the last decade a substantial amount has been published addressing the nonlinear static response of laminated beams, plates, and shells with attached piezoelectric devices subjected to thermoelectromechanical loads. The reported works implement various types of external loads, kinematic assumptions, and numerical methods to solve the resultant nonlinear equations. [Tzou and Zhou \[1997\]](#) reported theoretical work on the dynamics, electromechanical coupling, and control of thermal buckling of a nonlinear piezoelectric laminated circular plate with an initial large deformation, [Bao et al. \[1998\]](#) analyzed nonlinear piezothermoelastic laminated beams, and [Oh et al. \[2001\]](#) studied thermopiezoelectric phenomena of active laminated plates. [Wang et al. \[2004\]](#) analyzed adaptive structures involving large imposed deformation. [Ahmad et al. \[2004\]](#) formulated a nonlinear model of a smart beam using general electrothermoelastic relations. In [\[Varelis and Saravanos 2004\]](#) the present authors demonstrated the prebuckling and postbuckling response of piezoelectric plates solving the static coupled nonlinear equations, and in [\[Varelis and Saravanos 2008\]](#) we developed a coupled nonlinear shell element for the prediction of stable and unstable deflection paths of piezolaminated shells subject to thermoelectromechanical loads, and also demonstrated the capability of piezoelectric shells to induce large deflections through active snap-through buckling.

Keywords: adaptive structures, composite, piezoelectric, actuators, sensors, finite element, nonlinear dynamics, vibration, geometric nonlinearity, thermal, buckling.

Additional reported works addressed the nonlinear dynamic behavior of piezolaminated plates and beams limited, however, to small amplitude free vibrations. Lee and Lee [1997] investigated the linearized vibration behavior of unstiffened and stiffened thermally postbuckled anisotropic plates, Singha et al. [2006] predicted the vibration characteristics of thermally stressed skew plates, and Park and Kim [2006] investigated small amplitude vibration behavior of simply supported FGM plates with temperature dependent materials in prebuckling and postbuckling state. Oh et al. [2000] presented an uncoupled layerwise theory to quantify the influence of buckling and postbuckling on natural frequencies. In [Varelis and Saravanos 2006] we reported on a coupled nonlinear finite element for the prediction of small amplitude free vibrations of piezocomposite beams and plates subjected to large deflections and initial stresses and quantified the advantages of the coupled formulation; a strong relation between modal frequencies and the ongoing buckling prediction was also postulated.

Very little work has been reported on the nonlinear dynamic response of adaptive piezoelectric structures for large loads and deflection amplitudes. Gao and Shen [2003] adopted first-order shear deformation theory for analyzing the geometrical nonlinear transient vibration response of plates and their control. Yi et al. [2000] applied solid elements to perform geometrically nonlinear analysis of surface bonded piezoelectric sensor wafers on plates and shells. Mukherjee and Chaudhuri [2005] developed a finite element for piezolaminated beams using an uncoupled approach for the prediction of sensory voltage in polyvinylidene fluoride (PVDF) bimorph cantilever beams vibrating at large amplitudes. Lentzen et al. [2007] worked on the control of the nonlinear vibration of piezoelectric beams under transverse load. Oh [2005] developed a finite plate element encompassing an uncoupled layerwise theory considering snap-through piezoelectric behavior.

The current paper presents a nonlinear coupled thermopiezoelectric plate theory and a finite element for laminated piezoelectric plates undergoing large displacements and rotations, for predicting the nonlinear dynamic response of adaptive plates exposed to dynamic thermal, electrical, and mechanical loads. The coupled nonlinear governing equations for piezolaminates are first formulated using the mixed-field shear-layerwise kinematic assumptions [Varelis and Saravanos 2008]. Generalized governing equations are formulated combining the Green–Lagrange nonlinear strains, with the kinematic assumptions of the mixed-field shear-layerwise shell laminate theory and linear thermopiezoelectric constitutive equations, including rotational inertia effects. Based on the previous generalized mechanics, a local finite element approximation is formulated and an eight-node nonlinear thermopiezoelectric plate element is developed. Finally, the discrete nonlinear coupled dynamic equations of motion are solved at each time step using the Newmark time integration in combination with a Newton–Raphson technique. Validation cases verify the present model, and various numerical examples evaluate the capability of the present method to predict the oncoming dynamic instability of smart beams under various combinations of dynamic mechanical, electric, and thermal loads.

2. Piezoelectric laminated shells

The case of a piezoelectric laminate plate is considered, consisting of an arbitrary configuration of linear piezoelectric layers or composite plies. The material of each ply of the piezoelectric laminate is assumed to remain within the range of linear piezoelectricity,

$$\sigma_i = C_{ij}^{E,T} S_j - e_{ik}^T E_k - \lambda_{im}^{E,T} \theta_m, \quad D_l = e_{lj}^T S_j + \varepsilon_{lk}^{S,T} E_k + p_{lm}^T \theta_m, \quad (1)$$

where $i, j = 1, \dots, 6$ and $k, l = 1, \dots, 3$; σ_i and S_i denote the mechanical stresses and Green's engineering strains in extended vectorial notation, C_{ij} is the elastic stiffness tensor, e_{ik} is the piezoelectric tensor, E_k is the electric field vector, λ_{im} is the thermal expansion tensor, $\theta_m = \Delta T = T - T_o$ is the temperature difference between the current temperature T and the thermally stress-free reference temperature T_o , D_l is the electric displacement vector, ε_{lk} is the electric permittivity tensor, and p_{lm} is the pyroelectric tensor. Superscript E, S, T represent constant voltage, strain, and temperature conditions, respectively.

The first shear deformation theory for the elastic displacements in combination with a layerwise linear field assumption for the electric potential and temperature are implemented, in the context of the mixed-field kinematic assumptions. Geometric nonlinear effects are usually realized in flexible structures which do not exhibit significant shear deformable effects, and vice versa; therefore, the consideration of shear deformation mainly aims to improve to the robustness of the linear part of the solution at plates of higher thickness aspect ratios.

The mechanical strains, the electric and thermal field components through the thickness of the laminate take the form

$$S_i = S_i^o + zk_i^o + S_{Li} \quad (i = 1, 2, 6), \quad S_{sj} = S_{sj}^o \quad (j = 4, 5), \quad (2)$$

where S_i^o and S_{sj}^o are the midsurface in-plane and shear strains respectively, k_i^o are the midsurface curvatures, and S_{Li} the resultant nonlinear mechanical strains described with respect to midsurface parameters:

$$S_{L1} = \frac{1}{2} w_{,x}^o{}^2, \quad S_{L2} = \frac{1}{2} w_{,y}^o{}^2, \quad S_{L6} = w_{,x}^o w_{,y}^o. \quad (3)$$

The generalized electric fields are

$$E_i(x, y, z, t) = \sum_{i=1}^m E_i^m(x, y, t) \Psi^m(z) \quad (i = 1, 2), \quad E_3(x, y, z, t) = \sum_{i=1}^m E_3^m(x, y, t) \Psi_{,z}^m(z). \quad (4)$$

The generalized thermal field is

$$\Theta(x, y, z, t) = \sum_{m=1}^N \Theta^m(x, y, t) \Psi^m(z), \quad (5)$$

where N indicates the number of discrete layers which may subdivide the laminate, E^m and Θ^m are the generalized electric and thermal fields at the m discrete layer, $\Psi^m(\zeta)$ are linear interpolation functions, and N is the number of discrete layers.

2.1. Generalized dynamic equations of motion in variational form. Since the present formulation refers to dynamic generalized equations, the estimation of the latter from a known equilibrium configuration at discrete time t to the next equilibrium state in discrete time $t + \Delta t$ is required. Through the use of the divergence theorem and neglecting the damping effects, the generalized imbalances between external and internal mechanical forces and electric charges, away from the equilibrium denoted by the vectors Ψ_u and Ψ_e , can be expressed at time t over the volume of the piezoelectric laminated plate, in an equivalent variational form:

$$\begin{aligned} \delta u^T {}^t\Psi_u &= - \int_V \delta {}^tS^T {}^t\sigma dV + \int_V \delta u^T {}^t b dV - \int_V \delta u^T \rho {}^t\ddot{u} dV + \int_{\Gamma_r} \delta u^T {}^t\bar{\tau} d\Gamma, \\ \delta \phi^T {}^t\Psi_e &= - \int_V \delta {}^tE^T {}^t\mathcal{D} dV + \int_{\Gamma_q} \delta \phi^T {}^t\bar{q} d\Gamma, \end{aligned} \quad (6)$$

where tS and ${}^t\sigma$ are the total Green–Lagrange strain tensor and second Piola–Kirchhoff stress tensor respectively, tb are the body forces, $\rho {}^t\ddot{u}$ indicate the inertia body forces, ${}^t\tau$ are the surface tractions on the bounding surface Γ_τ , tq is the electrical charge applied on the terminal bounding surface Γ_q , an overbar indicates surface quantities, and V represents the whole laminated plate volume including all passive and active piezoelectric layers.

Substituting Equations (1)–(5) into (6), integrating over the thickness coordinate ζ and collecting the mechanical, electric, and thermal field state variables, the following generalized equations of motion result, which express the electromechanical equilibrium of the laminate at time step t :

$$\begin{aligned} \delta^t u^T {}^t\Psi_u = & - \int_{A_o} \left(\delta^t S^{oT} [A] {}^tS^o + \delta^t S^{oT} [B] {}^tk^o + \delta^t k^{oT} [B] {}^tS^o + \delta^t k^{oT} [D] {}^tk^o + \delta^t S_s^{oT} [A_s] {}^tS_s^o \right. \\ & + \delta^t S^{LT} [A] {}^tS^o + \delta^t S^{LT} [A] {}^tS^L + \delta^t S^{LT} [B] {}^tk^o + \delta^t S^{oT} [A] {}^tS^L + \delta^t k^{oT} [B] {}^tS^L + \sum_m \delta^t S^{oT} [\bar{E}^m] {}^tE^m \\ & + \sum_m \delta^t k^{oT} [\hat{E}^m] {}^tE^m + \sum_m \delta^t S^{LT} [\bar{E}^m] {}^tE^m + \sum_m \delta^t S^{oT} [\bar{\Theta}^m] {}^t\Theta^m + \sum_m \delta^t k^{oT} [\hat{\Theta}^m] {}^t\Theta^m \\ & \left. + \sum_m \delta^t S^{LT} [\bar{\Theta}^m] {}^t\Theta^m \right) dA + \int_{A_o} (\delta^t u^T b^A + \delta^t \beta^T b^B) dA + \int_{\Gamma_\tau} \delta^t \bar{u}^T t_\tau d\Gamma, \quad (7) \end{aligned}$$

$$\begin{aligned} \delta^t \phi^T {}^t\Psi_e = & - \int_{A_o} \left(\sum_m \delta^t E^{mT} [\bar{E}^m] {}^tS^o + \sum_m \delta^t E^{mT} [\bar{E}^m] {}^tk^o + \sum_m \delta^t E^{mT} [\bar{E}^m] {}^tS^L \right. \\ & \left. + \sum_{mn} \delta^t E^{mT} [G^{mn}] {}^tE^n + \sum_{mn} \delta^t E^{mT} [T^{mn}] {}^t\Theta^n \right) dA + \int_{\Gamma_q} \delta \bar{\phi}^T t_q d\Gamma, \quad m, n = 1, \dots, N, \end{aligned}$$

where $[A]$, $[B]$, $[D]$, and $[A_s]$ are the extensional, coupling, flexural, and shear stiffness matrices; E^m overbar and overhat are the equivalent extensional and flexural piezoelectric coefficients; $[\bar{\Theta}^m]$ and $[\hat{\Theta}^m]$ are the in-plane and out-of-plane laminate thermal expansion matrices; and G^{mn} are the generalized electric permittivity matrices.

3. Finite element methodology

In order to solve the above generalized nonlinear variational equation (7), the finite element methodology is adopted. The multifield state variables are approximated on the reference midplane A_o with local interpolation functions, taking the form

$$\begin{aligned} u_j^o(x, y, t) = & \sum_{i=1}^M u_j^{oi}(t) P^i(x, y) \quad (j = 1, 2, 3), \quad \beta_j^o(x, y, t) = \sum_{i=1}^M \beta_j^i(t) P^i(x, y) \quad (j = 1, 2), \\ \phi^m(x, y, t) = & \sum_{i=1}^M \phi^{mi}(t) P^i(x, y) \quad \text{and} \quad \theta^m(x, y, t) = \sum_{i=1}^M \theta^{mi}(t) P^i(x, y) \quad (m = 1, \dots, N), \end{aligned} \quad (8)$$

where N indicates the number of discrete layers which subdivide the laminate, M the number of element nodes, and P denotes local C_o continuous interpolation functions.

3.1. Generalized dynamic equations of motion in variational form. Substituting (8) into (7) and collecting the common nodal displacement, electric potential, and temperature terms, the following coupled

system of nonlinear equations of motion is ultimately derived for time t :

$$\begin{aligned} {}^t\Psi_u(u, \varphi) &= [M]{}^t\ddot{u} + [K_{uu}(u, \varphi)]{}^t u + [K_{ue}(u, \varphi)]{}^t \varphi + [K_{u\theta}(u, \varphi)]{}^t \theta - {}^t R = 0, \\ {}^t\Psi_e(u, \varphi) &= [K_{eu}(u, \varphi)]{}^t u + [K_{ee}(u, \varphi)]{}^t \varphi + [K_{e\theta}(u, \varphi)]{}^t \theta - {}^t Q = 0, \end{aligned} \tag{9}$$

where ${}^t u$ and ${}^t \phi$ are the nodal displacement and electric potential vectors, respectively, and ${}^t \theta$ is the applied nodal temperature vector ${}^t \theta = \{ {}^t \theta^A \}$; ${}^t R$ and ${}^t Q$ are the externally applied mechanical loads and charge vectors at time t , respectively. The electric potential vector ${}^t \phi$ encompasses both applied and free electric potential terms, that is

$${}^t \phi = \begin{bmatrix} {}^t \phi^A \\ {}^t \phi^S \end{bmatrix},$$

where ${}^t \phi^A$ is the externally applied nodal electric potential at the actuators and ${}^t \phi^S$ is the induced unknown electric potential at nodes with prescribed electric displacement. In a smart piezoelectric plate, the electric potential vectors ϕ^A and ϕ^S correspond to actuators and sensors respectively, moreover, in case of an adaptive structure they may be further connected through a proper controller; however, in this study no feedback from sensors to actuators is considered. At mechanical and electrical equilibrium, where ${}^t\Psi_u = 0$ and ${}^t\Psi_e = 0$, equations (9) represent the discrete system of nonlinear equilibrium equations and the electric potential ϕ^S together with the free displacement nodal vector u represents the unknowns of the nonlinear system. The availability of active and sensory electric potential in combination with the nonlinear system (9), reflects the capability of the present model to be interfaced in future studies through a nonlinear controller. The matrices $[K]$ with subscripts $uu, ue, ee, u\theta$, and $e\theta$ indicate the actual stiffness, piezoelectric, electric permittivity, thermal expansion, and pyroelectric matrices respectively, including linear and nonlinear terms:

$$\begin{aligned} [K_{uu}(u, \phi)] &= [K_{uu}^o] + [K_{uu}^L] = [K_{uu}^o] + [P_1(u)] + [P_2(u^2)], \\ [K_{ue}(u, \phi)] &= [K_{ue}^o] + [K_{ue}^L] = [K_{ue}^o] + [P_3(u)], \\ [K_{eu}(u, \phi)] &= [K_{eu}^o] + [K_{eu}^L] = [K_{eu}^o] + [P_4(u)], \\ [K_{ee}(u, \phi)] &= [K_{ee}^o]. \end{aligned} \tag{10}$$

3.2. Solution scheme for coupled nonlinear equations. Let us assume that an equilibrium between internal and external mechanical forces and electric charges has been predicted for the configuration at time t , yielding ${}^t\Psi_u = 0$ and ${}^t\Psi_e = 0$. Assuming also that external forces and charges are applied incrementally at discrete time steps, such that ${}^{t+\Delta t}R = {}^t R + \Delta R$ and ${}^{t+\Delta t}Q = {}^t Q + \Delta Q$, we are looking to predict the next equilibrium state at time $t + \Delta t$, which will satisfy the equilibrium equations ${}^{t+\Delta t}\Psi_u = 0$ and ${}^{t+\Delta t}\Psi_e = 0$. The resulting global set of generalized equations of motion are solved in time, using Newmark’s time integration method.

Since the imbalance forces and charges ${}^{t+\Delta t}\Psi_u(u, \phi)$ and ${}^{t+\Delta t}\Psi_e(u, \phi)$ depend nonlinearly on the nodal point displacements and electric potentials, convergence can’t be directly achieved at each time step. Thus, the Newton–Raphson iterative technique is adopted in order to solve the generalized nonlinear dynamic equations at each iteration, shown analytically below for the k -th iteration into the configuration

time $t + \Delta t$:

$$\begin{aligned} {}^{t+\Delta t}\bar{K}_{uu}(u^{k-1}, \phi^{k-1})\Delta u^k + {}^{t+\Delta t}\bar{K}_{ue}(u^{k-1}, \phi^{k-1})\Delta \phi^k &= -{}^{t+\Delta t}\Psi_u(u^{k-1}, \phi^{k-1}), \\ {}^{t+\Delta t}\bar{K}_{eu}(u^{k-1}, \phi^{k-1})\Delta u^k + {}^{t+\Delta t}\bar{K}_{ee}(u^{k-1}, \phi^{k-1})\Delta \phi^k &= -{}^{t+\Delta t}\Psi_e(u^{k-1}, \phi^{k-1}). \end{aligned} \tag{11}$$

In the above system of equations, the overbar indicates tangential structural, piezoelectric, and permittivity matrices which encompass the following matrix terms:

$$\begin{aligned} [\bar{K}_{uu}(u, \phi)] &= \frac{4}{\Delta t^2}[M] + [\bar{K}_{uu}^o] + [\bar{K}_{uu}^\sigma] + [\bar{P}_1(u)] + [\bar{P}_2(u^2)], \\ [\bar{K}_{ue}(u, \phi)] &= [\bar{K}_{ue}^o] + [\bar{K}_{ue}^L] = [\bar{K}_{ue}^o] + [\bar{P}_3(u)], \\ [\bar{K}_{eu}(u, \phi)] &= [\bar{K}_{eu}^o] + [\bar{K}_{eu}^L] = [\bar{K}_{eu}^o] + [\bar{P}_4(u)], \\ [\bar{K}_{ee}(u, \phi)] &= [\bar{K}_{ee}^o]. \end{aligned} \tag{12}$$

The updated displacement, velocity, acceleration, and electric potential vectors are expressed below:

$$\begin{aligned} {}^{t+\Delta t}u^{(k)} &= {}^{t+\Delta t}u^{(k-1)} + \Delta u^{(k)}, \\ {}^{t+\Delta t}\dot{u}^{(k)} &= \frac{4}{\Delta t^2}({}^{t+\Delta t}u^{(k-1)} - {}^t u) - \frac{4}{\Delta t} {}^t \dot{u} - {}^t \ddot{u}, \\ {}^{t+\Delta t}\phi^{(k)} &= {}^{t+\Delta t}\phi^{(k-1)} + \Delta \phi^{(k)}, \end{aligned} \tag{13}$$

where ${}^t u$, ${}^t \dot{u}$, and ${}^t \ddot{u}$ are the converged values at time step t related to the respective values at step $t + \Delta t$ as follows: ${}^t u = {}^{t+\Delta t}u^{(0)}$, ${}^t \dot{u} = {}^{t+\Delta t}\dot{u}^{(0)}$, and ${}^t \ddot{u} = {}^{t+\Delta t}\ddot{u}^{(0)}$.

4. Numerical results

Validation and novel evaluation cases of the developed FE model are presented, for various active piezoelectric laminated beams and plates under combined thermoelectromechanical dynamic loading conditions. The considered materials were aluminum, graphite-epoxy, PVDF piezopolymer, and PZT5 piezoceramic, the properties of which are shown in [Table 1](#).

5. Validation cases

5.1. Mechanical buckling of a cantilever bimorph beam under ramp loading. In the present numerical case the lateral nonlinear dynamic response of a PVDF [p/p] bimorph cantilever beam was examined. The beam was 100 mm long and 5 mm wide and the thickness of the PVDF layer was 0.5 mm. A ramp point load of 0.005 N was applied in the transverse direction at the middle of the tip along with a constant uniform axial mechanical load. Closed circuit electric conditions were considered at each piezoelectric layer. [Figure 1](#) shows the transverse deflection amplitude on the tip versus time, when a compressive axial load is applied. Obviously the displacement amplitude increases as the axial compressive load approaches the critical value $F_{cr} = 0.204$ N, due to softening effects. Also the curves corresponding to higher compressive loads exhibit a higher vibration period due again to the reduction of stiffness. Conversely, [Figure 2](#) illustrates the tip vibration of the beam subject to a tensile axial load and shows an amplitude reduction with a simultaneous vibration period reduction due to stiffening effects produced by

Property	Gr/epoxy	Al	PZT-5	PVDF	Property	Gr/epoxy	Al	PZT-5	PVDF
Elastic properties (10^9 Pa)					Electric permittivity (10^{-9} F/m)				
E_{11}	132.4	66	62	2	ϵ_{11}	0.031	0.026	23	0.1
E_{22}	10.8	66	62	2	ϵ_{22}	0.026	0.026	23	0.1
E_{33}	10.8	66	62	2	ϵ_{33}	0.026	0.026	24	0.1
G_{23}	3.6	27	23.6	0.77	Thermal expansion coefficient (10^{-6} / $^{\circ}$ C)				
G_{13}	5.6	27	23.6	0.77	α_{11}	-0.9	24	1.1	42
G_{12}	5.6	27	18	0.77	α_{22}	27	24	1.1	42
ν_{12}	0.24	0.3	0.31	0.29	Pyroelectric constant (10^{-3} / m^2 $^{\circ}$ C)				
ν_{13}	0.24	0.3	0.31	0.29	p_{11}	0	0	-0.2	0.05
ν_{23}	0.49	0.3	0.31	0.29	p_{22}	0	0	-0.2	0.05
Piezoelectric coefficients (10^{-12} m/V)					p_{33}	0	0	-0.2	0.05
d_{31}	0	0	-220	-16					
d_{32}	0	0	-220	-16					
d_{24}	0	0	670	33					
d_{15}	0	0	670	33					

Table 1. Material properties. All E and G values in units of GPa.

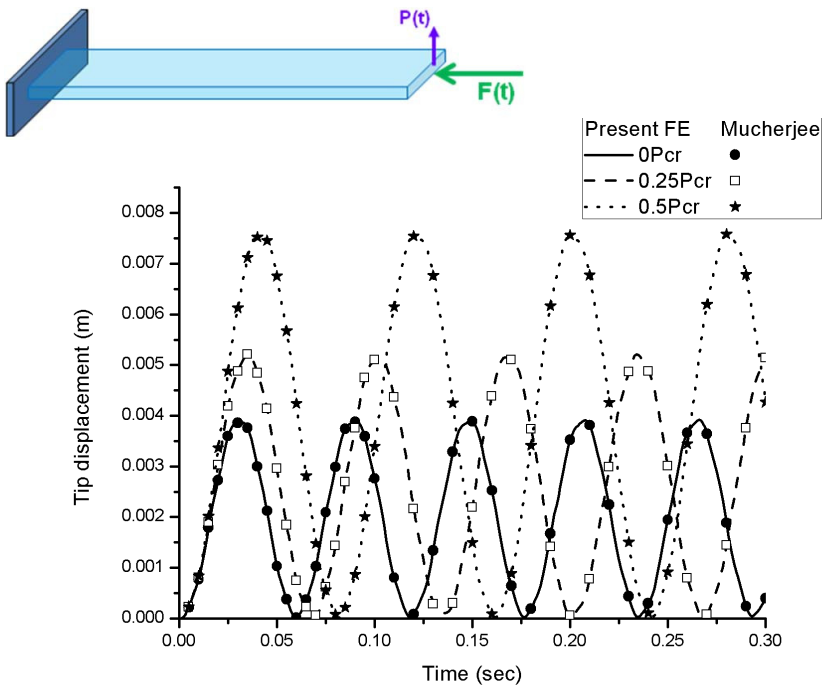


Figure 1. Tip dynamic displacement of a bimorph [PVDF/PVDF] cantilever beam induced by a combined step in-plane compressive and ramp transverse load applied at the tip of the beam.

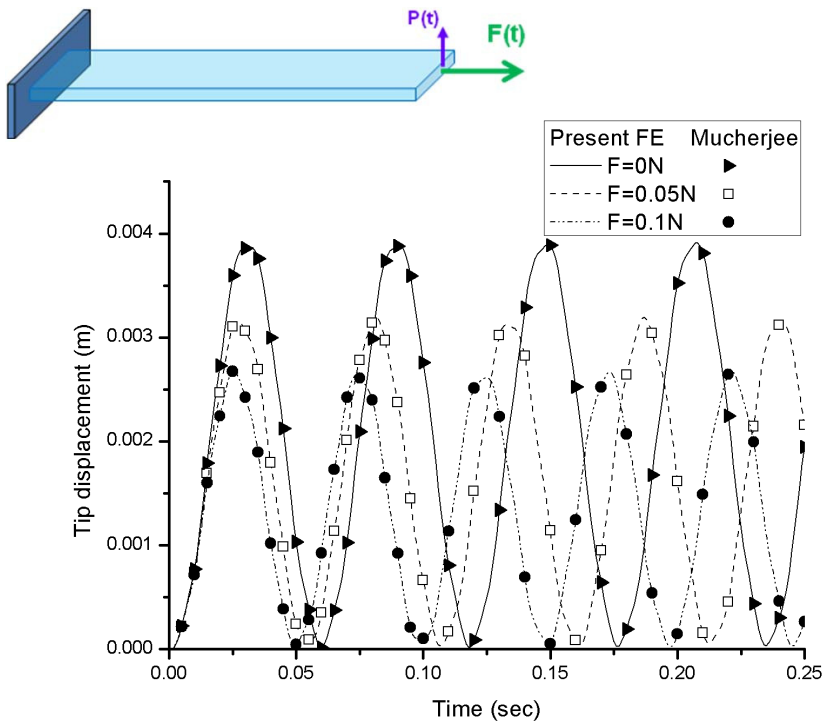


Figure 2. Tip dynamic displacement of a bimorph [PVDF/PVDF] cantilever beam induced by a combined ramp transverse and step in-plane tensile mechanical load applied at the tip of the beam.

the axial tensile load. Finally, the results are in excellent agreement with those reported by [Mukherjee and Chaudhuri \[2005\]](#) who used a beam finite element based on uncoupled laminate theory.

5.2. Fully simply-supported square plate under pulse loading. In the second validation case, the dynamic response of a fully simply supported square $2.438 \text{ m} \times 2.438 \text{ m}$ aluminum plate, with thickness 6.35 mm was investigated. A uniform pressure pulse load $P = 47.84 \text{ Pa}$ was applied on the plate. An 8×8 element mesh model was used. [Figure 3](#) shows the dynamic response of the plate under various pulse load values. The results reveal the nonlinear dependence between applied load and vibration amplitude and period due to membrane effects. The predicted results are in excellent agreement with those reported by [Gao and Shen \[2003\]](#), who used an uncoupled piezoelectric laminate theory and a four node plate finite element. Overall, the current method has accurately predicted the nonlinear dynamic response of flexible structures including the onset of dynamic mechanical buckling, as well as the stiffening effects due to tensile axial loads.

6. Numerical examples

6.1. Mechanical buckling of a cantilever bimorph beam under various ramp loads. The nonlinear dynamic response of a cantilever [PVDF/PVDF] beam, having the same geometric dimensions with that of the first validation case is further studied. Three compressive ramp loads with identical maximum

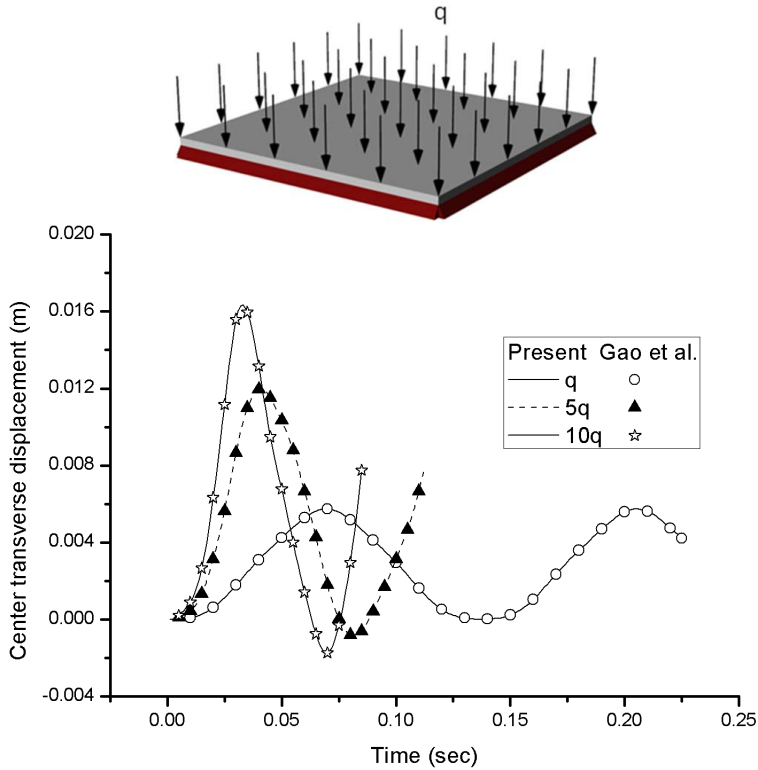


Figure 3. Central dynamic transverse deflection of a square simply-supported aluminum plate loaded under various uniform step pressures.

values $F_{\max} = 1.1F_{\text{cr}}$ ($F_{\text{cr}} = 0.204 \text{ N}$), were progressively applied at the tip of the beam however, at different rates (see Figure 4a). A step of low uniform pressure (0.5 Pa) was applied on the beam at $t = 0 \text{ sec}$ in order to induce an eccentricity and a stable buckling path (see Figure 4a). Figure 4b shows the transverse displacement at the tip of the beam versus the time for the various ramp load rates. Clearly all three curves show a rapid increase of the dynamic tip deflection near the corresponding buckling load step, which however occurs at different times for each loading rate, with the high-rate ramp load reaching the critical buckling load faster, and so forth. Yet, the rate of loading is predicted to have a drastic effect on the resultant maximum dynamic tip deflection. Apparently, in the high-rate ramp load inertial forces also play a dominant role in the dynamic buckling of the beam, and vice versa. The predicted results show the capability of the method to predict the onset of dynamic buckling under various dynamic loads.

6.2. Active thermopiezoelectric buckling of a simply-supported composite beam. The nonlinear dynamic response of a simply-supported $[p/0/90/45/-45]_s$ graphite/epoxy beam with continuous piezoelectric layers attached on the upper and lower surface is predicted. The length and the width of the beam were 200 mm and 20 mm, respectively; the thicknesses of the composite plies and piezoelectric layers were $h_l = h_p = 0.1 \text{ mm}$. The beam is loaded by a time step of uniform temperature load ΔT applied at $t = 0 \text{ sec}$, and a ramp piezoelectric load with rate $dV/dt = 600 \text{ V/sec}$, induced by unidirectional electric fields imposed by equal but opposite in polarity electric potential values applied on the outer terminals of

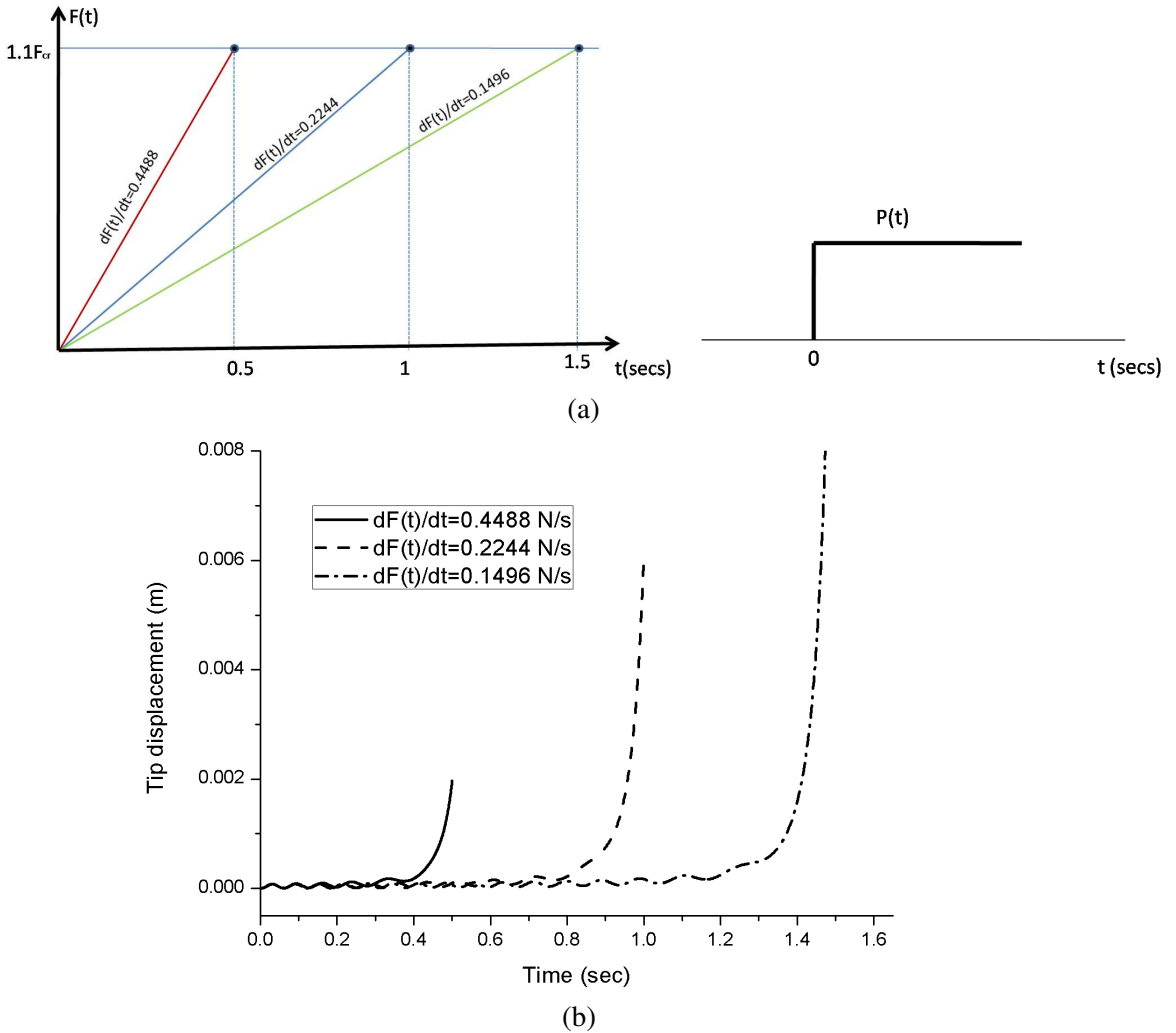


Figure 4. Effect of the rate of an in-plane compressive ramp force on the onset of dynamic buckling of a bimorph [PVDF/PVDF] cantilever beam. (a) Time dependence of applied loads and (b) predicted transverse tip displacement.

the piezoactuators (see Figure 5a). An imperfection induced by a time step of very low constant uniform pressure (1 Pa) was considered to stimulate the onset of a stable buckling path (see Figure 5a). Figure 5b shows the predicted center transverse displacement of the beam versus time. Both thermal load and electric fields induce in-plane compressive stresses in the beam. The beam buckles under the piezoelectric load alone ($\Delta T = 0^\circ\text{C}$), but the simultaneous application of the thermal load effectively causes the shifting of the stable equilibrium trajectory. The underlying vibration on the buckling trajectory is caused by the lateral force and near and beyond the critical electric potential the vibration amplitude reaches higher values due to the initiation of dynamic buckling. The results show the inherent capability of the present method to simulate the combined dynamic thermoelectric buckling of flexible piezocomposite structures.

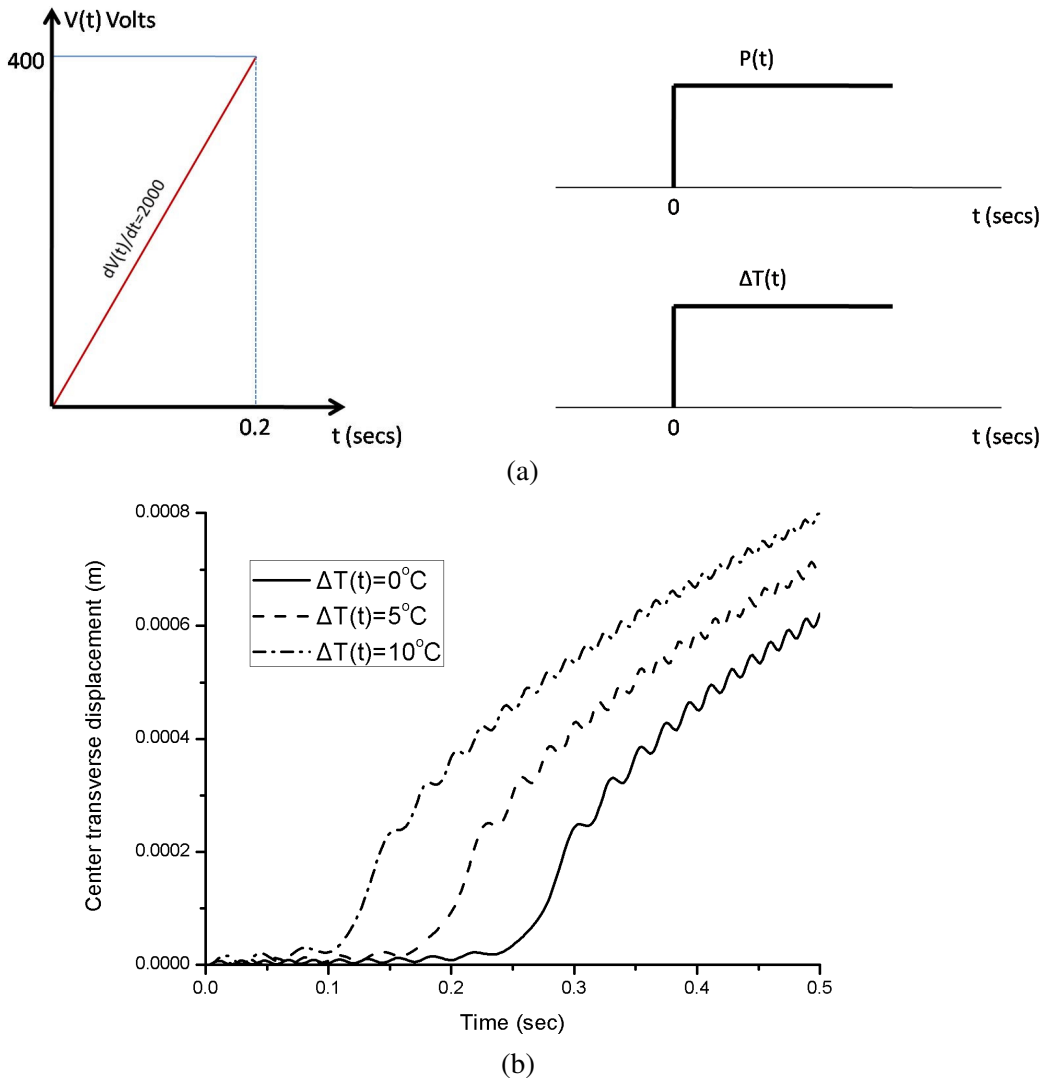


Figure 5. Dynamic buckling response of a simply-supported active $[p/0/90/45/-45]_s$ beam under combined uniform in-plane piezoelectric, in-plane thermal, and off-plane pressure loads. (a) Time dependence of applied electric field, temperature, and uniform pressure; and (b) predicted transverse deflection at center.

6.3. Laminated active beam under electromechanical bending load. In the present case, the bending response of a simply-supported active $[p/0/90/45/-45]_s$ gr-epoxy beam subject to combination of dynamic electromechanical loads is simulated. The geometric dimensions of the beam are the same as those of the previous example. A time step of uniform pressure (200 Pa) was applied on the beam at $t = 0$ sec (see Figure 6a). A uniform and equal in value and polarity ramp electric potential was also imposed on the outer terminals at each piezoelectric layer at $t = 0$ sec, while their inner terminals remained grounded, such that distributed piezoelectric bending moment was progressively induced on

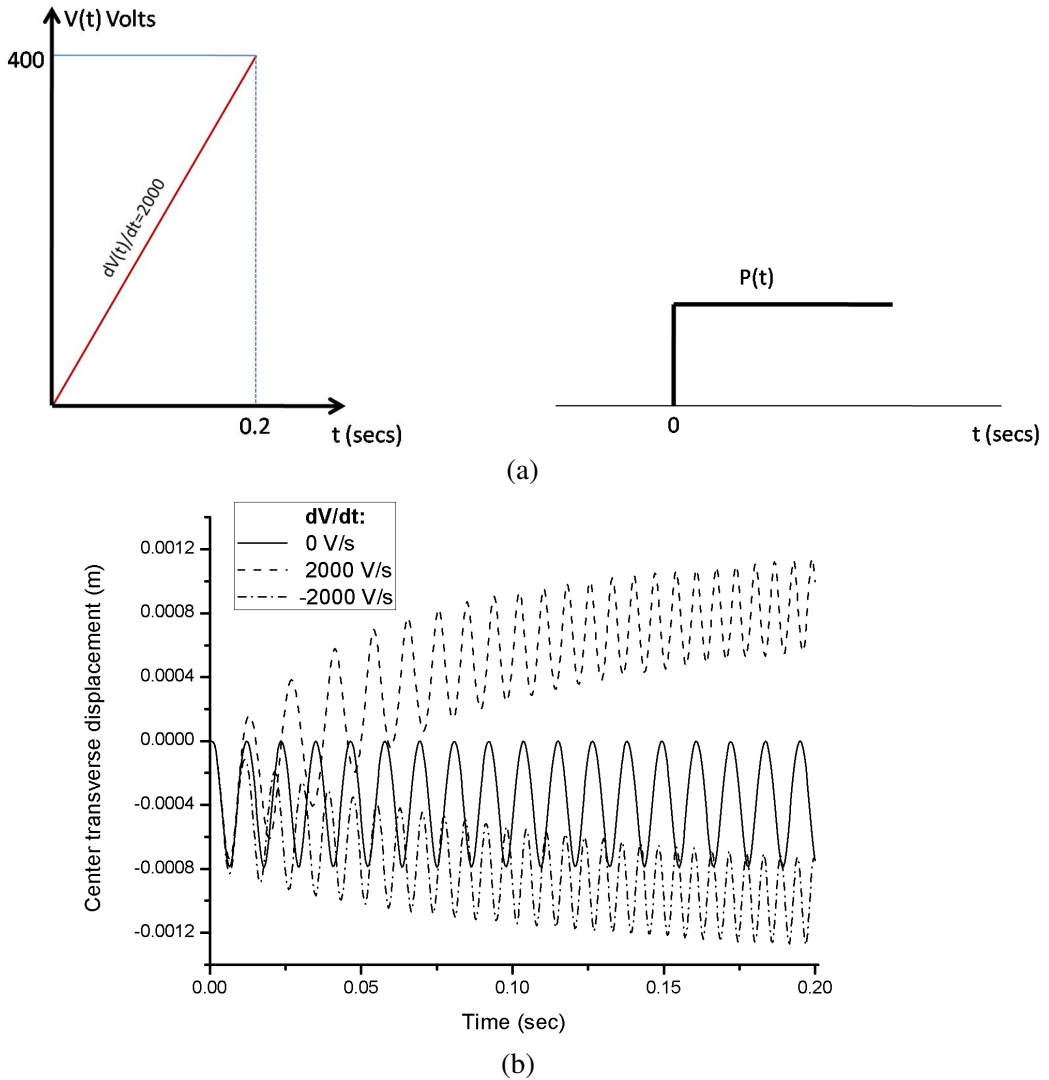


Figure 6. Bending of a simply-supported active $[p/0/90/45/-45]_s$ beam under a combined bending piezoelectric load with a uniform pressure. (a) Time dependence of applied loads, and (b) transverse deflection at center.

the beam (see Figure 6a). Figure 6b shows the predicted transverse displacement at midspan versus time for three cases of ramp electric loads: $V_{\max} = 0$ V, $dV/dt = 0$ V/sec; $V_{\max} = 400$ V, $dV/dt = 2000$ V/sec; and $V_{\max} = -400$ V, $dV/dt = -2000$ V/sec. The free vibration is caused mainly by the applied time step of uniform pressure. The curves corresponding to positive and negative electric potential, show great differences in the vibratory response and the underlying average displacement, indicating strong nonlinearity in the respective response.

6.4. Active buckling of simply-supported composite beam under combined thermopiezoelectric loading. The dynamic response of a simply-supported $[p/0/90/45/-45]_s$ gr-epoxy beam with continuous

piezoelectric actuators attached on the upper and lower surface is predicted. The length and the width of the beam were 200 mm and 20 mm, respectively; the thicknesses of the composite plies and piezoelectric layers were $h_l = h_p = 0.1$ mm. The beam is loaded by a step of uniform temperature thermal load ΔT , a ramp piezoelectric load ($V_{\max} = 2V_{\text{cr}}$, $dV/dt = 110$ V/sec), inducing unidirectional electric fields in the piezoactuators through the application of equal but opposite electric potential values on their outer terminals, and a time step of very low constant uniform pressure (3 Pa), all applied at $t = 0$ sec (see Figure 7a). Both the thermal and the piezoelectric loading induce in-plane compressive stresses in the beam. The predicted thermal and electric potential critical values were $\Delta T_{\text{cr}} = 18^\circ\text{C}$ and $V_{\text{cr}} = 54$ V respectively. Figures 7b and 7c show the predicted dynamic center transverse displacement of the beam

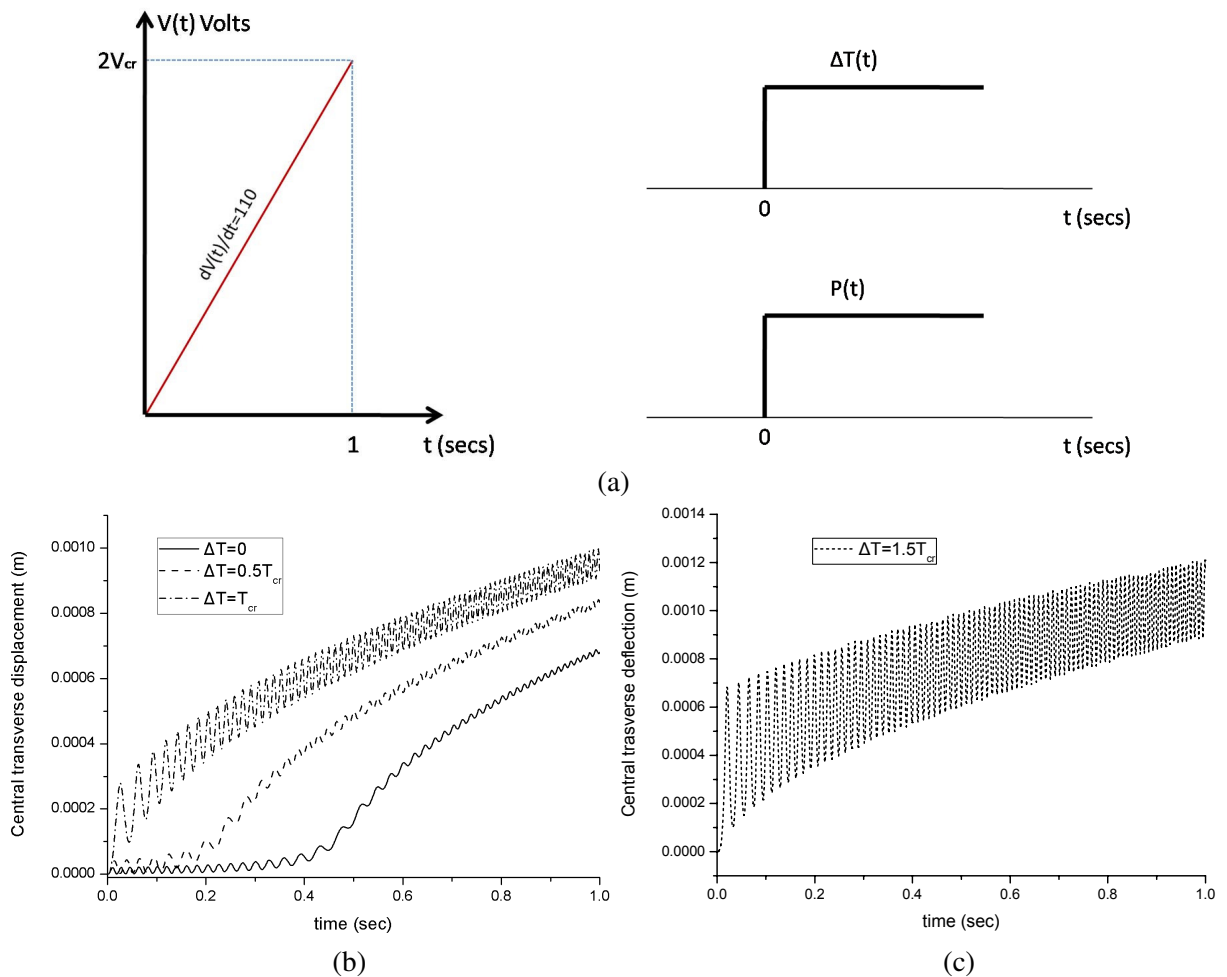


Figure 7. Dynamic thermopiezoelectric buckling of a simply-supported active $[\text{p}/0/90/45/-45]_s$ beam under combined compressive in-plane piezoelectric and thermal loading and small uniform pressure (a) time dependence of applied loads; (b) and (c) predicted center deflection for various thermal load values.

versus time for thermal load values. Without thermal buckling load ($\Delta T = 0^\circ\text{C}$) the beam enters in the pure piezoelectric buckling under compressive stresses caused by the piezoelectric actuators. All other trajectories are the result of combined application of various temperature loads ΔT and approach earlier the onset of buckling due to additional compressive thermal stresses. Obviously, for $\Delta T = T_{cr}$ and $1.5T_{cr}$, the beam buckles first thermally and due to the loss of its out-of-plane stiffness vibrates under much higher amplitudes. Again, the results show the inherent capability of the present method to simulate the combined dynamic thermoelectric buckling of flexible piezocomposite structures.

7. Summary and conclusions

A theoretical framework and a finite element methodology were presented, to predict the coupled nonlinear dynamic response of active laminated piezoelectric beams and plates exposed to dynamic thermoelectromechanical fields. The mechanics uses the mixed-field shear-layerwise laminate kinematic assumptions and encompasses the geometric nonlinearity due to large displacements and rotations. An eight-node nonlinear coupled plate element was developed. The coupled generalized nonlinear dynamic equations of motion were formulated, linearized, and solved using the Newton–Raphson technique in combination with the Newmark time integration method.

Validations and evaluation cases of laminated beams and plates subject to high in-plane and out-of-plane dynamic loads demonstrated the capability of the present method to accurately and robustly predict their nonlinear dynamic response. Moreover they quantified the complex and highly nonlinear dynamic response of active structures.

The obtained numerical results illustrate the tendency of active plate beams to exhibit substantially different behavior under dynamic loads than static buckling. In this context, the rates of applied loads drastically affect the dynamic buckling trajectory, and vibrations may coexist which change the amplitude and frequency near critical loads. Thermal loads may significantly influence the highly nonlinear response of piezocomposite beams shifting the stable equilibrium trajectory due to additional compressive/tensile thermal stresses. The possibility of actively inducing large vibration amplitudes by combining steady external mechanical or thermal loads with proper dynamic electric potential input on the actuators was also quantified.

References

- [Ahmad et al. 2004] S. N. Ahmad, C. S. Upadhyay, and C. Venkatesan, “Linear and nonlinear analysis of a smart beam using general electrothermoelastic formulation”, *AIAA J.* **42**:4 (2004), 840–849.
- [Bao et al. 1998] Y. Bao, H. S. Tzou, and V. B. Venkayya, “Analysis of non-linear piezothermoelastic laminated beams with electric and temperature effects”, *J. Sound Vib.* **209**:3 (1998), 505–518.
- [Gao and Shen 2003] J.-X. Gao and Y.-P. Shen, “Active control of geometrically nonlinear transient vibration of composite plates with piezoelectric actuators”, *J. Sound Vib.* **264**:4 (2003), 911–928.
- [Lee and Lee 1997] D.-M. Lee and I. Lee, “Vibration behaviors of thermally postbuckled anisotropic plates using first-order shear deformable plate theory”, *Comput. Struct.* **63**:3 (1997), 371–378.
- [Lentzen et al. 2007] S. Lentzen, P. Klosowski, and R. Schmidt, “Geometrically nonlinear finite element simulation of smart piezolaminated plates and shells”, *Smart Mater. Struct.* **16**:6 (2007), 2265–2274.
- [Mukherjee and Chaudhuri 2005] A. Mukherjee and A. S. Chaudhuri, “Nonlinear dynamic response of piezolaminated smart beams”, *Comput. Struct.* **83**:15–16 (2005), 1298–1304.

- [Oh 2005] I.-K. Oh, “Thermopiezoelectric nonlinear dynamics of active piezolaminated plates”, *Smart Mater. Struct.* **14**:4 (2005), 823–834.
- [Oh et al. 2000] I.-K. Oh, J.-H. Han, and I. Lee, “Postbuckling and vibration characteristics of piezolaminated composite plate subject to thermo-piezoelectric loads”, *J. Sound Vib.* **233**:1 (2000), 19–40.
- [Oh et al. 2001] I.-K. Oh, J.-H. Han, and I. Lee, “Thermopiezoelectric snapping of piezolaminated plates using layerwise nonlinear finite elements”, *AIAA J.* **39**:6 (2001), 1188–1198.
- [Park and Kim 2006] J.-S. Park and J.-H. Kim, “Thermal postbuckling and vibration analyses of functionally graded plates”, *J. Sound Vib.* **289**:1–2 (2006), 77–93.
- [Singha et al. 2006] M. K. Singha, L. S. Ramachandra, and J. N. Bandyopadhyay, “Vibration behavior of thermally stressed composite skew plate”, *J. Sound Vib.* **296**:4–5 (2006), 1093–1102.
- [Tzou and Zhou 1997] H. S. Tzou and Y. H. Zhou, “Nonlinear piezothermoelasticity and multi-field actuations, 2: Control of nonlinear deflection, buckling and dynamics”, *J. Vib. Acoust. (ASME)* **119**:3 (1997), 382–389.
- [Varelis and Saravanos 2004] D. Varelis and D. A. Saravanos, “Coupled buckling and postbuckling analysis of active laminated piezoelectric composite plates”, *Int. J. Solids Struct.* **41**:5–6 (2004), 1519–1538.
- [Varelis and Saravanos 2006] D. Varelis and D. A. Saravanos, “Small-amplitude free-vibration analysis of piezoelectric composite plates subject to large deflections and initial stresses”, *J. Vib. Acoust. (ASME)* **128**:1 (2006), 41–49.
- [Varelis and Saravanos 2008] D. Varelis and D. A. Saravanos, “Non-linear coupled multi-field mechanics and finite element for active multi-stable thermal piezoelectric shells”, *Int. J. Numer. Methods Eng.* **76**:1 (2008), 84–107.
- [Wang et al. 2004] D. W. Wang, H. S. Tzou, and H.-J. Lee, “Control of nonlinear electro/elastic beam and plate system: finite element formulation and analysis”, *J. Vib. Acoust. (ASME)* **126**:1 (2004), 63–70.
- [Yi et al. 2000] S. Yi, S. F. Ling, and M. Ying, “Large deformation finite element analyses of composite structures integrated with piezoelectric sensors and actuators”, *Finite Elem. Anal. Des.* **35**:1 (2000), 1–15.

Received 6 Jul 2009. Revised 26 Aug 2009. Accepted 4 Sep 2009.

DIMITRIS VARELIS: barell@mech.upatras.gr

Applied Mechanics Section, Department of Mechanical Engineering and Aeronautics, University of Patras, 26500 Patras, Greece

DIMITRIS SARAVANOS: saravanos@mech.upatras.gr

Applied Mechanics Section, Department of Mechanical Engineering and Aeronautics, University of Patras, 26500 Patras, Greece